DESIGN AND ANALYSIS OF PITCH-TYPE SINGLE SEEDING TEST PLATFORM

, *俯仰式播种单体试验台设计与分析*

Yi-fei LI¹⁾, Yi-kai LI¹⁾, Tian-min YI²⁾, Shu-juan YI*¹⁾

¹⁾ College of Engineering, Heilongjiang Bayi Agricultural University, Daqing, Heilongjiang/ China
²⁾ College of Basic Education, Beijing Polytechnic University, Beijing/ China
Tel: +86-459-13836961877; E-mail: yishujuan_2005@126.com
Corresponding author: Shu-juan Yi
DOI: https://doi.org/10.35633/inmateh-77-39

Keywords: Profiling mechanism; Testing platform; Hydraulic system; RecurDyn simulation

ABSTRACT

To address the difficulty in evaluating the performance of the seeding unit profiling mechanism, a pitching testing platform for examining seeding units with profiling mechanisms was designed. The main system and key component parameters of the testing platform were determined, and a hydraulic system was developed to overcome the challenge of simulating field undulation curves. The feasibility of the hydraulic and transmission systems was verified using RecurDyn dynamic simulation technology. The simulation results showed that the hydraulic system of the testing platform could effectively reproduce wave curves at different speeds, with a maximum roller stress of 46.61 MPa and a maximum strain of -73.99 × 10-6. To further evaluate the actual performance of the testing platform, the seeding unit of the Debont 1205 high-speed no-till corn planter was used as the test object. Using the average adjustment time and average adjustment accuracy as evaluation indicators, parameters were collected at operating speeds of 2.22 m/s, 2.78 m/s, and 3.33 m/s, and compared with those obtained from the testing platform. The test results revealed that the maximum error in the detection of average adjustment time was 0.27 s, and the maximum error in the detection of average adjustment accuracy was 2.58 × 10-3 m. These findings indicate that the testing platform can effectively evaluate the regulation performance of the profiling mechanism at different operating speeds and provide an accurate indoor platform for testing seeding units.

摘要

"针对播种单体仿形机构性能缺乏有效检测手段的问题,本研究开发了一套专用于带仿形机构播种单体的室内投掷性能检测平台。该平台的关键在于设计并集成了液压系统,以精准模拟田间复杂的地面起伏轮廓。研究详细阐述了平台的核心构成系统及关键部件的参数设定。为验证方案可行性,利用 RecurDyn 动力学仿真技术对液压与传动系统进行了建模分析,结果表明: 平台液压系统能有效复现不同行进速度下的起伏地形波浪曲线; 关键滚筒部件的最大应力为 46.61 MPa, 最大应变值为-73.99x 10⁻⁶,均处于安全范国内。为评估平台的实际检测效能,选用 Debont 1205 高速免耕玉米播种机的播种单体作为测试对象。在实际田间作业中(2.22m/s、2.78m/s、3.33m/s 速度下),采集了仿形机构的平均调节响应时效和平均调节精度作为基准指标。将这些指标与在检测平台上获取的对应数据进行比较。对比测试结果显示: 检测平台测得的平均调节时间最大误差为 0.27 秒; 平均调节精度的最大检测误差为 2.58×10⁻³米。此结果证明,该检测平台能够可靠地评估不同作业速度下仿形机构的动态调节性能,成功构建了一个精确的室内测试环境,为播种单体的性能检测提供了有效解决方案。"。

INTRODUCTION

The consistency of seeding depth is an important factor to improve the yield and quality of maize (Walne et al., 2022; Bazzaz et al., 2018; Romaneckas et al., 2009; Helios et al., 2021). With the improvement of the accuracy requirements about seeding, the profiling mechanism of planter, which is used to improve the consistency of seeding depth, has gradually generated the demand for the development of profiling performance (Liu et al., 2022; Cai et al., 2011). However, the operation of profiling mechanism in the field is complicated, which means it is not easy to accurately monitor the profiling performance of the seeding unit, let alone carry out tests related to the optimization of profiling performance. In order to meet this demand, many scholars have conducted their studies related to seeding unit test bench (Zhou et al., 2023; Gao et al., 2020).

Tang et al., (2017), designed a testing platform that simulates ground undulations through the combined operation of a load-bearing plate and a floating mechanism. The system employed a dual hydraulic cylinder structure equipped with sensors to effectively reproduce ground undulations and collect profiling performance data. Tang et al. (2021) designed a seeding unit testing platform capable of simulating sinusoidal undulation curves. Using high-speed camera technology, the platform was able to analyze the performance of the combined machine under different forward speeds. Cao et al., (2022), developed an active profiling device and designed a seeding unit downforce testing bench based on the 2BMZF corn planter to verify its accuracy. This testing bench could collect and record planter downforce in real time. In the same year, Ding et al., (2022), designed a seeding unit field test bench that could simulate both undulating terrain and forward operation conditions, enabling detection of the profiling performance of the seeding unit during low-speed operation in specific plots.

However, research on seeding unit testing platforms still has limitations in accurately simulating the operating environment of the unit and in acquiring profiling performance data. In this study, a pitching testing platform for examining seeding units with profiling mechanisms was designed by coordinating the transmission system with the hydraulic system to simulate the working conditions of the seeding unit. In addition, a sensor monitoring system was developed to collect profiling performance data of the seeding unit and to calculate the regulation accuracy and regulation speed of the profiling mechanism based on these data. The rationality of the testing platform design was verified using RecurDyn dynamic simulation technology, and the accuracy of its detection performance was validated through comparison with actual field test data. This study provides an indoor testing platform for evaluating the profiling mechanisms of seeding units, meeting the requirements for profiling performance testing and promoting the development of active profiling technology.

MATERIALS AND METHODS

Experimental Setup

(1) Seeding Unit Structure

The seeding unit with a profiling mechanism is the main working component of the testing platform. The overall structure of the seeding unit is shown in Figure 1. The seeding unit typically consists of a weeding wheel, stubble cutter, slotted tray, paddle wheel, suppressing wheel, and a profiling mechanism (*Ma et al., 2023*). During operation, under the traction of a tractor, the seeding unit sequentially performs furrow opening, seeding, fertilizing, covering, and pressing (*Yi et al., 2024*). In this process, the profiling mechanism, utilizing its motion characteristics, adjusts the seeding depth when encountering ground undulations (*Hou et al., 2024*; *Liu et al., 2024*). Due to its unique ability to improve the consistency of seeding depth, the profiling mechanism is a key component of the seeding unit (*Bai et al., 2020*).

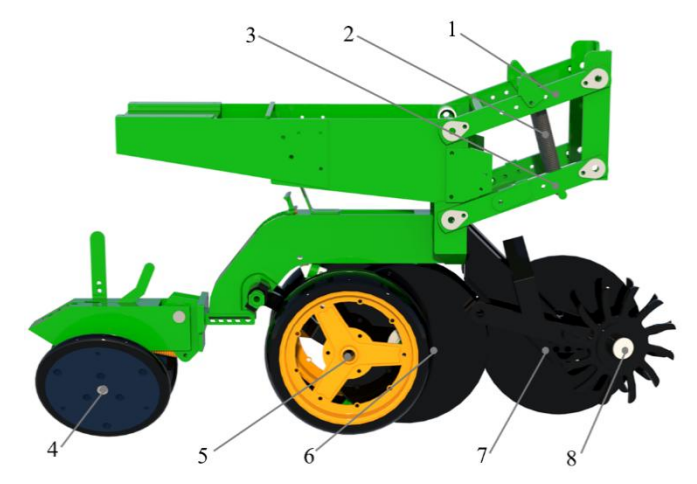


Fig. 1 - Overall structure of seeding unit

Upper Profiling Bar;
 Profiling Springs;
 Lower Profiling Bar;
 Suppressing Wheel;
 Paddle Wheel;
 Slotted Tray;
 Stubble Cutter;
 Weeding Wheel

(2) Testing Platform Overview

The overall structure of the pitching testing platform for examining seeding units with profiling mechanisms is shown in Fig. 2. The platform mainly consists of the overall frame, power system, hydraulic system, transmission system, and sensor monitoring system.

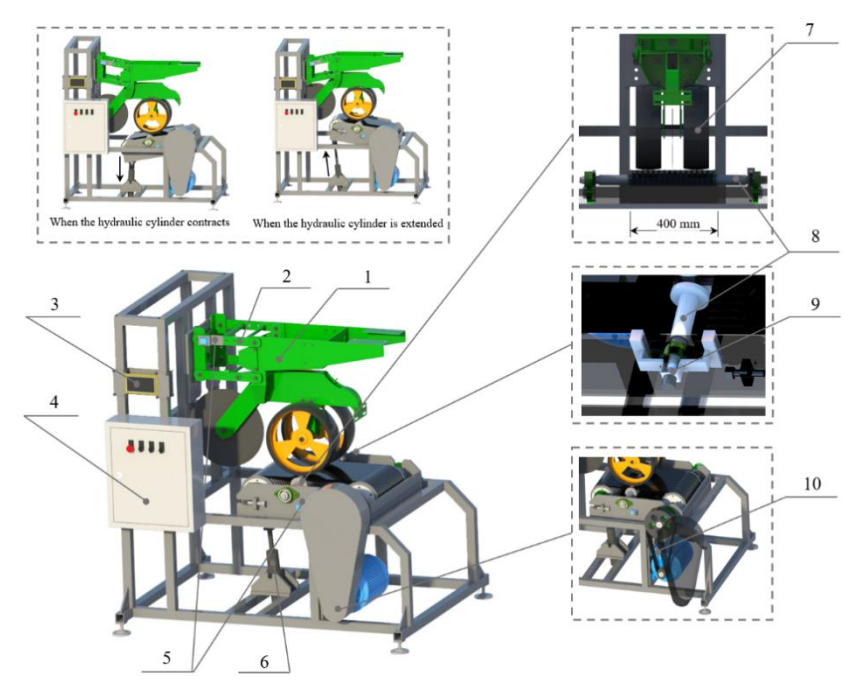


Fig. 2 - Structural diagram of the pitching testing platform for examining the seeding unit with a profiling mechanism

1. Seeding Unit; 2. Profiling mechanism; 3. Vehicle-mounted computers; 4. Button module; 5. Angle Sensor; 6. Hydraulic system; 7. Ballast wheel; 8. Roller; 9. Optical encoder; 10. Transmission system

The power system mainly consists of a motor and a frequency converter; the hydraulic system mainly consists of a hydraulic cylinder and a hydraulic pump; the transmission system mainly consists of pulleys, platform frame, V-belts, V-belt rollers, and roller; the monitoring system mainly consists of computer, angle sensors, and optical encoder. The motor is fixed to the bottom of the assembly frame and is connected to a small pulley. The small pulley is connected to a large pulley via A Type V-belts. The large pulley is fixed to the drive roller on the pitch platform and is coaxial with the double-ear bearing housing. The hydraulic lifting system is located on the overall frame and is connected to the lower end of the pitch platform. Two angle sensors are installed on the side of the pitch platform and on the profiling mechanism of the seeding unit, respectively. The optical encoder is installed on the roller, and the computer and control box are located on the side of the frame. Additionally, two belt tensioning devices are located on the motor mounting plate and on both sides of the pitch platform. The performance indicators of the testing platform are shown in Table 1.

Table 1

Parameter	Number	
Overall dimensions (L×W×H) /(m×m×m)	1.735×1.296×1.772	
Matching power/kW	3	
Pitching platform speed/(m·s-1)	2.09~5.35	
Tilt angle of pitching platform/($^{\circ}$)	-12~9	
Lifting height of pitching platform/m	-0.063~0.051	

When the testing platform needs to be run, the seeding unit is fixedly connected to the testing platform though an installation plate, and the ground undulation curve of a specific plot at a certain operating speed is input into the onboard computer as target terrain data in text form. During operation, the onboard computer controls the motor to drive the V-belts and the large pulley. The large pulley rotates coaxially with the active V-belt roller on the pitch platform, and the V-belt starts to transmit, reaching the corresponding speed, thus simulating the high-speed forward operation state of the seeding unit under the traction of a tractor. At the same time, the computer controls the hydraulic system in real-time based on the target terrain data. The hydraulic system is equipped with a throttle valve and an electromagnetic relief valve. The computer controls the hydraulic components to achieve precise regulation of the piston rod's extension amount and speed, thereby simulating the target undulation curve.

Also, the angle sensors located on the profiling mechanism of the seeding unit and the pitch platform, and the optical encoder located on the roller, collect relevant data in real-time as the testing bench operates. The collected data is used to determine the contouring amount of the profiling mechanism, the simulated undulation amount of the testing bench, and the forward speed of the seeding unit, which are displayed on the screen. The difference between the contouring amount and the simulated undulation amount is the adjustment error P_t (m), which can intuitively represent the regulation accuracy of the profiling mechanism. Using a 5-second regulation interval, the time difference required for the profiling mechanism to reach the same undulation curve extremum as the simulated undulation amount within the same regulation interval is the adjustment time T_t (s). The adjustment time can intuitively represent the regulation speed of the profiling mechanism of planter.

Mechanical Design

The transmission system of testing platform uses a motor with a power of 3.3 kW, a voltage of 380 V, and a speed of 1450 r/min. Due to the small center distance and high speed of the testing bench, the transmission system is designed to use V-belt drives. V-belt drives have the advantages of a large range of center distance variation, smooth transmission, and easy maintenance.

The testing platform mainly consists of large pulley, small pulley, A Type V-belt, motor, and the pitch platform. The pitch platform is a key component of the testing bench, designed with a pitch structure for elevation. It primarily comprises active V-belt roller, roller, C Type V-belt, rollers, and pitch platform tensioning device. Its function is to drive the paddle wheels of the seeding unit through the transmission of 15 C Type V-belts, simulating the forward movement of the seeding unit.

Taking the soil in northern China as an example, the soil is generally lighter on the surface and more clayey below, with the surface primarily consisting of clay loam, and the friction coefficient ranging from 0.2 to 0.5. The outer surface material of the C Type V-belt is rubber, with a friction coefficient ranging from 0.3 to 0.5. Therefore, the C Type V-belt is used to simulate high-speed field operations (*Jiu et al., 2023*). The specific structure of the transmission system of the testing platform is shown in Figure 3.

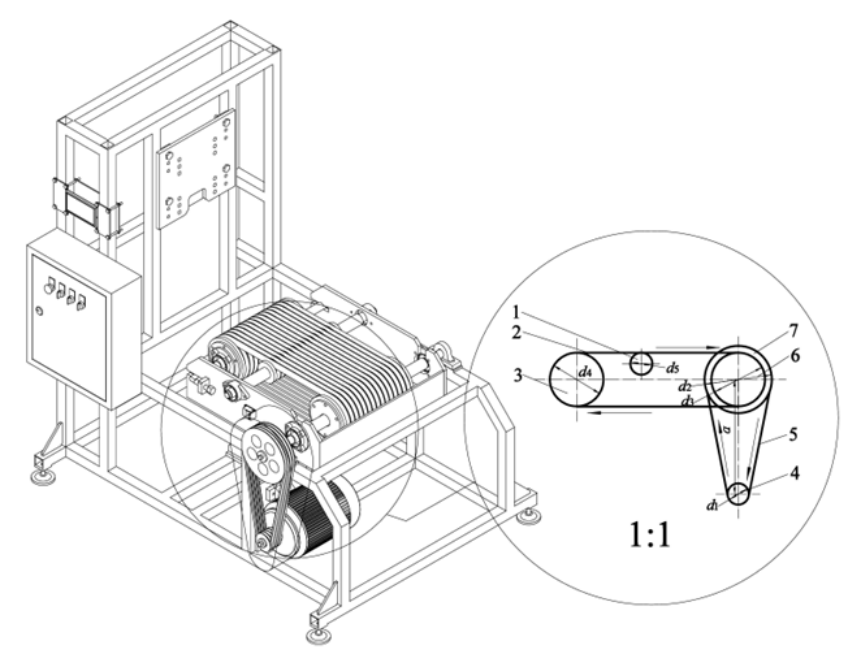


Fig. 3 – Schematic of testing platform belt drive and its drive principle

1. Roller; 2. C Type V-belt; 3. Passive V-belt roller; 4. Small pulley; 5. A Type V-belt; 6. Passive V-belt roller; 7. Large pulley

The design parameters were as follows: small pulley diameter d_1 =0.08m, large pulley diameter d_2 =0.25m, active V-belt roller diameter d_3 = 0.20 m, driven V belt roller diameter d_4 =0.20 m, and roller diameter d_5 =0.1m.

The center distance between the large and small belt pulleys is a= 0.4835 m. Accordingly, the small belt pulley speed R_1 (r/min), the large belt pulley speed R_2 (r/min), the active roller speed R_3 (r/min), the driven roller speed R_4 (r/min), roller speed n_5 (r/min), and the linear speeds of the A-type V-belt v_0 (m/s) and C-type V-belt v_1 (m/s) are determined as described by w and w and w are determined as described by w and w are w and w are determined as described by w and w are w and w and w are w

$$\begin{cases}
R_1 = R_0 \\
R_2 = R_3 = R_4 = \frac{R_0 d_1}{d_2} \\
R_5 = \frac{R_0 d_1 d_3}{d_2 d_5} \\
v_0 = \frac{\pi d_1 R_1}{60} \\
v_1 = \frac{\pi d_4 R_2}{60}
\end{cases} \tag{1}$$

where: n_0 - motor speed, (r/min).

Taking China as an example, the forward speed of domestically produced air-suction planters with more than six rows is currently about 3.33 m/s, while some high-speed planters can reach speeds of up to 5 m/s. Considering the current development trend toward high-speed and precision planting, the designed testing platform should achieve a maximum transmission speed ν_1 of no less than 5.28 m/s to meet the performance testing requirements of the seeding unit. Under different gears of the frequency converter, R_0 ranges from 625 to 1595 r/min. Substituting these values into Equation (1) yields a conveyor speed for the pitching platform ranging from 2.09 to 5.35 m/s, which satisfies the design requirements.

The testing platform transmission ratio i is calculated as:

$$i = \frac{R_0}{R_2} \tag{2}$$

Substituting n_0 =1595 r/min, n_3 =510 r/min into Equation (2), gives i = 3.2. Since $2 \le i \le 4$, the transmission ratio of the testing platform's transmission system is appropriate.

The wrap angle refers to the angular contact between the belt and pulley, denoted by the symbol α_1 . In general, the wrap angle should satisfy $\alpha_1 \ge 120^\circ$. Considering the weight of a single unit and its operating speed, a wrap angle of $\alpha_1 \ge 150^\circ$ is required.

The formula for calculating the wrap angle is:

$$\alpha_1 \approx 180^{\circ} - \frac{57.3^{\circ}}{a} (d_2 - d_1)$$
 (3)

Substituting the values of d_1 , d_2 and a into Equation (3), yields a wrap angle of the motor belt drive of α_1 =159.85°. Since $\alpha_1 \ge 150$ °, the design meets the required specification.

The main role of the tensioning device is to make the V-belt obtain the necessary initial tension to ensure the normal operation of the pitching platform. As shown in Figure 4, the pitching platform tensioning device is located at both ends of the driven roller, and the tensioning degree can be adjusted by rotating the bolt to change the shaft distance.

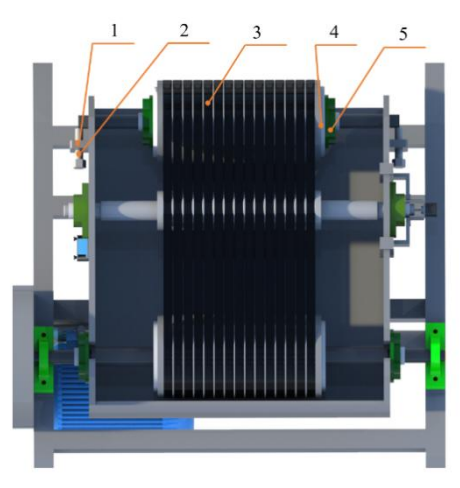


Fig. 4 – Schematic of the structure of the pitching platform tensioning device.

1. Double-ear bearing housing; 2. Earplug; 3. C type V-belt; 4. Passive V-belt roller; 5. Bear

The initial tension of the drive belt is the tension applied by the tensioning device when installing the drive belt and is expressed by the symbol F_0 (N). If the initial tension is too small, it will cause the V-belt to slide or even fall off, and if the initial tension is too large, it will increase the wear of the transmission system or even cause the V-belt to break. The formula for calculating the initial tension F_0 of a single V-belt on a pitching platform is as follows (Sun et al., 2021)

$$F_0 = q_c v_1^2 + 500 \frac{(2.5 - K_a) P_{ca}}{K_a Z_v v_1}$$
 (4)

where: K_a - wrap angle coefficient, taken as 1; P_{ca} - power, (kW); Z_v - the number of roots of V-belt; q_c - the mass of single C type V-belt per unit length, taken as 0.3 kg/m.

Substituting P_{ca} = 3.3 kW, Z = 15, and v_1 = 5.28m/s into Equation (5) yields F_0 = 39.6 N.

Hydraulic System Modeling

The hydraulic control schematic of the testing platform is shown in Figure 5.

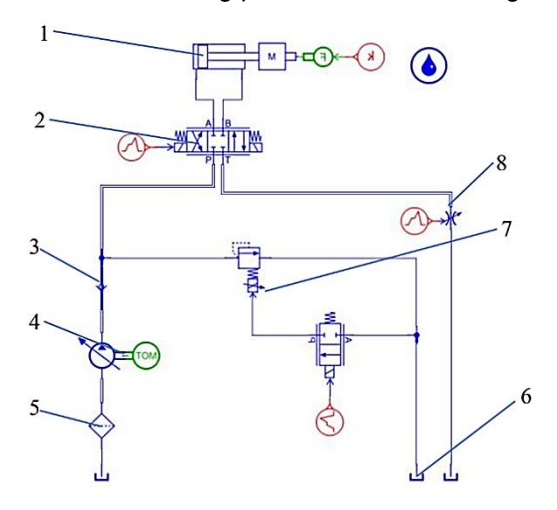


Fig. 5 – Schematic of testing platform hydraulic system

Hydraulic cylinder;
 3/4-way solenoid directional control valve;
 Check valve;
 Variable displacement pump;
 Hydraulic filter;
 Hydraulic oil tank;
 Pilot-operated solenoid relief valve;
 Throttle valve

The hydraulic system is primarily designed to simulate ground undulations, and its operating cycle consists of four phases: fast-forward phase of the hydraulic tappet, stationary working phase, fast-return phase, and stop.

Considering the seeding speed, general ground undulation frequency, and the amplitude of undulation, the maximum feed speed of the hydraulic cylinder, as well as its fast-forward and fast-return speeds, were designed to be 0.08 m/s (Zhang et al., Z018). Let D denote the hydraulic cylinder pressure and D4 the hydraulic cylinder flow. The calculation formula for the fast-forward phase is as follows:

$$p = \frac{F_s}{A - A_0} + \frac{A_0}{A - A_0} P_b \tag{5}$$

$$q = (A - A_0) V_1 \tag{6}$$

The formula for calculating the working phase is:

$$p = \frac{F_s}{A} + \frac{A_0}{A} P_b \tag{7}$$

$$q=Av_h$$
 (8)

The formula for calculating the fast-return phase is:

$$p = \frac{F_s}{A_0} + \frac{A}{A_0} P_b \tag{9}$$

$$q = A_0 v_I \tag{10}$$

where:

 F_s - load, 736.8 N during the fast-forward or fast-return phases, and 2193.7 N during the working phase; A - effective area of the rodless chamber of the hydraulic cylinder, cm²; A_0 - effective area of the rod chamber of the hydraulic cylinder, m²; p_b - back pressure, taken as 0.5 MPa; v_I - fast-forward and fast-return speed, m/s; v_h - maximum feed speed, m/s.

By substituting $A = 1.963 \times 10^{-3}$ m², $A_0 = 1.347 \times 10^{-3}$ m², $v_i = 0.08$ m/s, $v_h = 0.08$ m/s into Eqs. (5)~(10) the pressure and flow rate for each working phase were obtained. The hydraulic cylinder power P can then be calculated as follows:

$$P=0.01667 \cdot pq$$
 (11)

The calculation results are shown in Table 2.

Table 2 Hydraulic cylinder pressure, flow rate, and power during different working phases

Working phase	Working pressure p / MPa	Flow rate q / (m³/s)	Power <i>P </i> kW
Tappet fast-forward	2.30	4.93 × 10 ⁻⁵	0.113
Working (stationary)	1.70	1.57 × 10⁻⁴	0.267
Fast-return	1.30	1.08 × 10 ⁻⁴	0.140

Based on these results, the design parameters of the hydraulic pump station were determined as follows: the system rated pressure is 6.0 MPa, and the hydraulic pump displacement was selected as 13 mL/r. The key component of the hydraulic system, the pilot-operated solenoid relief valve, is a DBW10 model, with a maximum flow rate of 250 L/min and an operating voltage of 24 V.

Sensor and Data Acquisition

(1) Sensor monitoring system components

The adjustment accuracy and speed of the profiling mechanism is an important index to test the adjustment performance of the profiling mechanism, which can be obtained through the monitoring system after the operation of the bench (*Ni et al., 2021*). As shown in Figure 5, the monitoring system of the testing platform mainly consists of a computer, DYL626S-type angle sensor, E6B2-CWZ1X2000-type photoelectric encoder, SD memory card and touch screen. Based on the target terrain undulation curve, the corresponding hydraulic cylinder piston-rod displacement and speed are calculated for curve simulation, and the hydraulic components are controlled accordingly to reproduce the ground undulation. The initial data collected by the sensor is combined with the measurement model by the monitoring system to obtain the required data, and the SD memory card saves the data and displays it on the computer interactive interface.

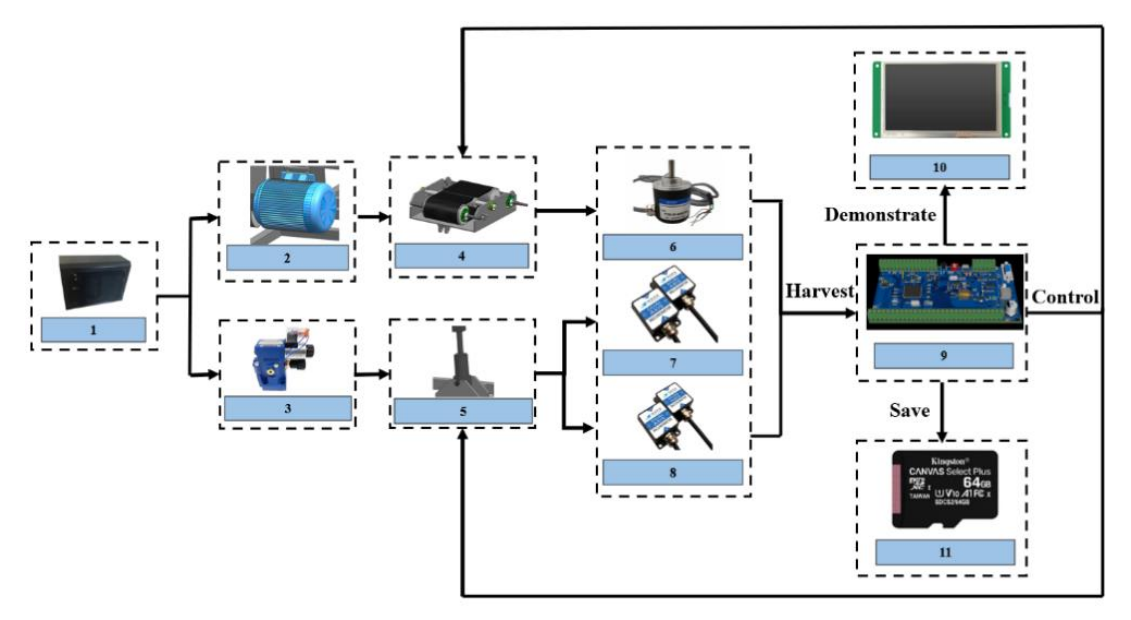


Fig. 6 – Schematic of testbench monitoring system

Computer; 2. Electrical machinery; 3. Pilot-operated solenoid relief valve; 4. Conveyor belts; 5. Hydraulic cylinder;
 Optical encoders for rollers; 7. Angle sensor for pitching platforms; 8. Angle sensor for profiling mechanism;
 Test bench monitoring system; 10. Human-computer interface; 11. SD memory card

The DYL626S angle sensor is located on the side of the pitching platform and on the parallelogram profiling mechanism. Take the angle sensor on the profiling mechanism as an example, the sensor will collect the angle change of the point where it is located, so as to calculate the actual profiling amount of the profiling mechanism as shown in Fig. 7.

(2) Monitoring system measurement model

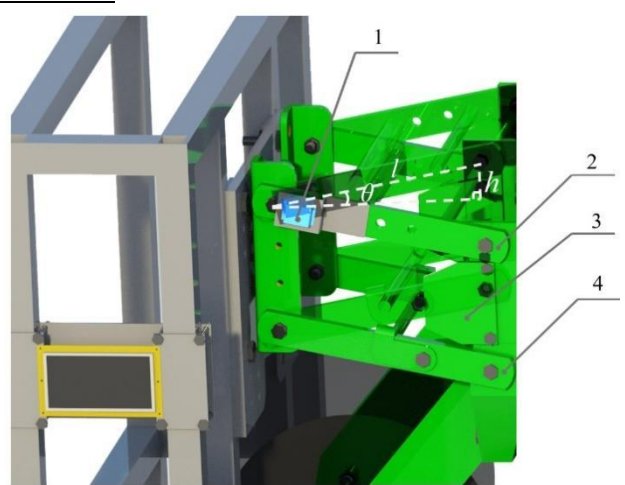


Fig. 7 – Schematic of angle sensor of profiling mechanism 1. Angle sensor; 2. Upper profiling bar; 3. Limit board; 4. Lower profiling bar

In Fig. 7, h is the required profiling amount of the profiling mechanism, m; θ is the angular change value collected by the angle sensor of the profiling mechanism, (°); l is the length of the connecting frame rod of the profiling mechanism, (m), which is a fixed value. Therefore, the obtained profiling amount h is:

$$h = \sin \theta \cdot l$$
 (12)

Similarly, the angle sensor mounted on the side of the pitching platform can be used to calculate the simulated heave of the platform, h_t (m), based on the measured change in the platform's angle. The calculation formula is as follows:

$$h_t = \sin \theta \ l_t \tag{13}$$

where: θ' - angle variation measured by the pitching platform angle sensor, (°); l_t - distance from the contact point between the seeding unit and the pitching platform to the vertical plane of the active V-belt roller axis, m.

By comparing the difference between the profiling displacement of the profiling mechanism and the simulated undulation h_t of the platform, the regulation accuracy of the profiling mechanism can be evaluated. Furthermore, by comparing the time difference between the profiling displacement h of the four-bar mechanism and the simulated undulation h_t of the platform at their final values, the regulation speed of the profiling mechanism can be assessed.

(3) Optical encoder measurement model

As shown in Figure 8, the E6B2-CWZ1X2000 photoelectric encoder is located on the rollers of the test stand to capture the rollers' rotational speed to calculate the conveyor belt speed v_1 .

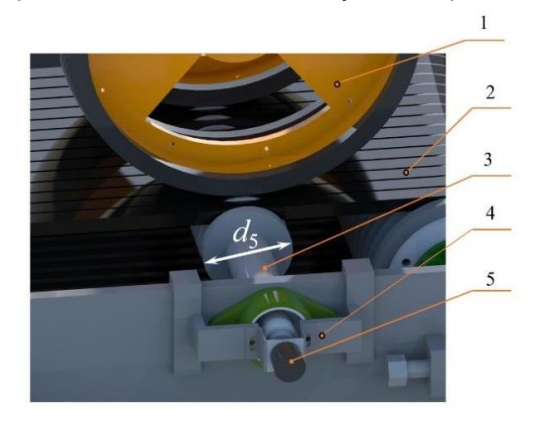


Fig. 8 – Schematic diagram of the optical encoder for the roller 1. Paddle wheel; 2. C type V-belt; 3. Roller; 4. Optical encoder fixtures; 5. Optical encoder

In the figure 8, d_5 represents the diameter of the roller, which is 0.1 m. Based on Equation (1), the C-type V-belt speed v_1 can be calculated as follows:

$$v_1 = \frac{\pi d_5 R_5}{60} \tag{14}$$

By calculating the conveyor belt speed V_1 , coordinated operation between the transmission system and the hydraulic lifting system can be achieved. This enables the simulation of forward motion at different operating speeds, as well as the corresponding undulation curves for each speed. As a result, the simulation more accurately reflects real field conditions and facilitates precise evaluation of the profiling performance of the seeding unit under various operating speeds.

Simulation Model

(1) Simulation Experiment and Analysis of the Testing Platform Based on RecurDyn

The testing platform simulates the ground undulations through the coordinated operation of hydraulic lifting and high-speed transmission. It is necessary to verify the rationality of the hydraulic system and transmission system design. This can be achieved through simulation experiments using multibody system simulation software like RecurDyn.

During the actual operation of the planter, the amplitude of the planter's undulation curve varies significantly at different operating speeds. Therefore, the simulation testing platform can be used to simulate the pitch restoration effect of the undulation curves at speeds of 2.22, 2.78, and 3.33 m/s, to test the stroke of the hydraulic system and the rationality of the pitching structure design of the testing platform.

Additionally, the structure of testing platform is relatively complex. During the coordinated operation of the hydraulic lifting system and high-speed transmission, certain stress and strain will inevitably be generated on the key components of the testing platform, especially the roller. The roller is a critical component of the testing platform frame, directly contacting the paddle wheel of the seeding unit during transmission. Besides collecting the V-belt speed of the testing platform, it also bears most of the weight of the seeding unit to prevent the V-belt from breaking. The pressure on the roller varies significantly depending on the simulated operating environment of the testing platform. Therefore, using RecurDyn to simulate the operating environment of the seeding unit at speeds of 2.22, 2.78, and 3.33 m/s, the stress and strain values of the key rollers can be obtained in real-time, to test the rationality of the testing platform transmission system design.

(2) Experimental Test and Analysis of the Testing Platform Based on Field Data

To validate the seeding performance of the seeding unit, field contour-following data were collected under different operating conditions and compared with corresponding bench test results. The experiments were conducted using the seeding unit of a Debont 1205 trailed no-till precision planter equipped with a spring-based contour-following mechanism. This unit is capable of high-speed seeding, meeting the requirements of the test. In addition, the spring profiling mechanism offers the advantages of short adjustment time and high adjustment accuracy; however, its profiling performance is significantly influenced by operating speed, making it highly suitable for validating the detection performance of the testing platform at three different working speeds.

Other major test equipment includes:

Tape measure (range 5 m, precision 1 mm)

Vernier caliper (range 150 mm, precision 0.01 mm)

Stopwatch (precision 0.01 s)

The test indicators for the testing platform are divided into two categories: adjustment accuracy detection and the adjustment time detection.

1) Test Indicators of Adjustment Accuracy Detection Error:

The adjustment accuracy detection error $\Delta_{\it F}$ (m) is defined as the difference between the adjustment error of the seeding unit profiling mechanism measured by the testing bench under a specific field terrain condition and the actual adjustment error of the unit during field operation. This difference reflects the accuracy of the testing bench in detecting the adjustment error of the seeding unit profiling mechanism. When the average error is consistently less than 3×10^{-3} m, the adjustment accuracy detection index is considered to meet the required standard.

2) Test Indicators of Adjustment Time Detection Error:

The adjustment time detection error, $\Delta \tau(s)$, is defined as the difference between the adjustment time of the seeding unit profiling mechanism measured by the testing bench under a specific field operating condition and the actual adjustment time of the unit during field operation. This difference reflects the accuracy of the

testing bench in detecting the adjustment time of the seeding unit profiling mechanism. When the average error is consistently less than 0.50 s, the adjustment speed detection accuracy index is considered to meet the required standard.

RESULTS AND ANALYSIS

Results of simulation test

The model was imported into RecurDyn, and the corresponding driving methods were configured. The driving methods for this testing platform mainly include the rotational drive of the transmission system and the linear displacement drive of the hydraulic system.

During the verification of the transmission system, the active V-belt roller was used as an example. The driving method was directly applied to the rotational joint of the active V-belt roller in RecurDyn. To more accurately simulate the actual startup conditions, a STEP time-step function was employed in this study. The expression of the function is as follows:

$$STEP(x, x_0, h_0, x_1, h_1)$$
 (15)

When x≤x₀

$$STEP = h_0 (16)$$

When $x_0 \le x \le x_1$

$$STEP = h_0 + (h_1 - h_0) \cdot \left[\frac{x - x_0}{x_1 - x_0} \right]^3 \cdot \left\{ 3 - 2 \left[\frac{x - x_0}{x_1 - x_0} \right] \right\}$$
 (17)

When x≥x1

$$STEP = h_1 \tag{18}$$

As an example, to simulate the operating environment of the seeding unit at a speed of 2.22 m/s using the testing platform, it was determined from Equation (2) that the rotational speed of the driven roller is 250 r/min. Therefore, the function expression for the actively driven roller is:

$$STEP(time, 0,0,0.1, -250)$$
 (19)

During the transmission process, the V-belt transmits motion through friction to drive the passive V-belt roller, roller, and paddle wheel. In this study, the Belt Toolkit was used to construct 15 V-belt models. The V-belt material was defined as rubber, and flexibility processing was applied to accurately simulate the power transmission characteristics of the testing platform's transmission system, as shown in Figure 9.

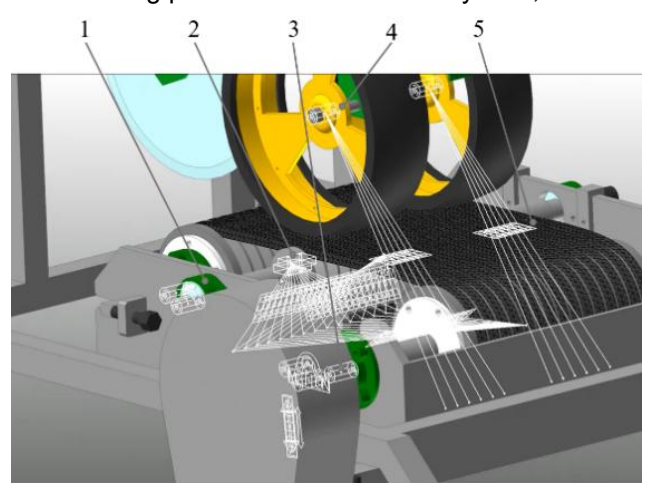


Fig. 9 – Flexibility modeling of the V-belt 1. Paddle wheel; 2. Rolls; 3. Passive V-belt roller; 4. Paddle Wheel; 5. C type V-belt

At the same time, the hydraulic system was validated. The testing platform simulates the field undulation curve of the seeding unit primarily through the extension and retraction of the hydraulic cylinder. The period of this curve is directly related to the operating speed of the planter in the field. In this simulation experiment, a sine function was used to represent the ground undulations, expressed as:

$$y = 25\sin(4\pi vt) \tag{20}$$

This simulation experiment reproduces the working state of the seeding unit at a speed of 2.22 m/s on the testing platform.

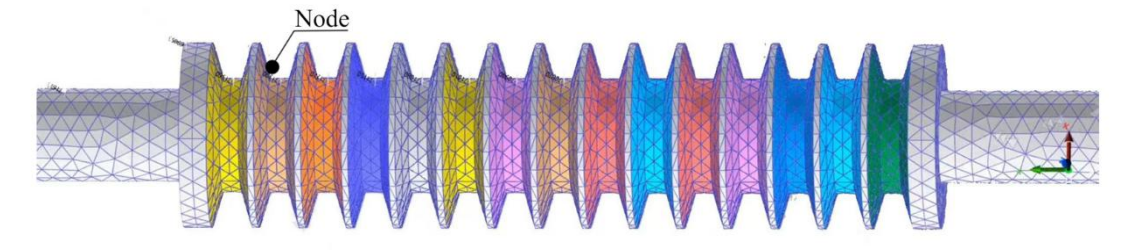
In RecurDyn, the driving method can be configured by adding a prismatic joint to the piston rod of the hydraulic cylinder and revolute joints at the hinge points of both the hydraulic cylinder and the platform. The periodic motion driving function used in this study is expressed as follows:

$$D = d * \left(\sin \left((2 * p_i)/t \right) * time \right) + \varphi \right)$$
 (21)

Based on Equation (19), the function expression for the piston rod motion is defined as follows:

$$25 * (\sin((10/4.5) * p_i * time))$$
 (22)

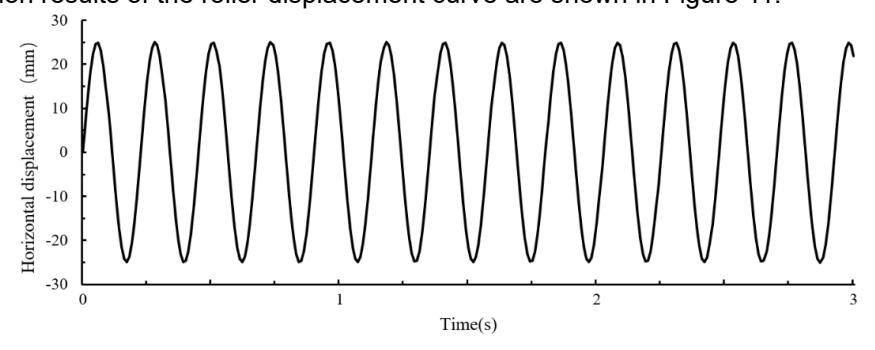
Additionally, during the lifting process, different lifting curves affect the stress-strain response of the roller. Therefore, this study employs the flexible body FFlex, which incorporates local stress-strain characteristics, to perform flexibility modeling of the roller. Node points were pre-defined at the contact positions between the roller and the paddle wheel to obtain displacement and pressure-strain curves at these locations, as shown in Fig.10.



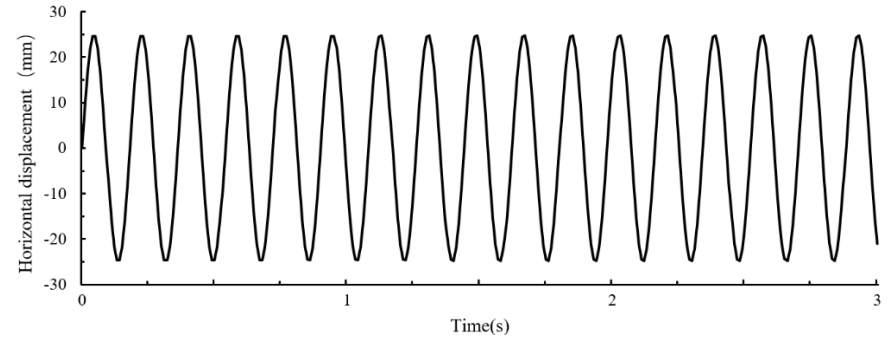
* Different colors represent the various grooved rollers, with the node located at the groove where the V-belt contacts the paddle wheel of the seeding unit.

Fig. 10 - Location of the node points

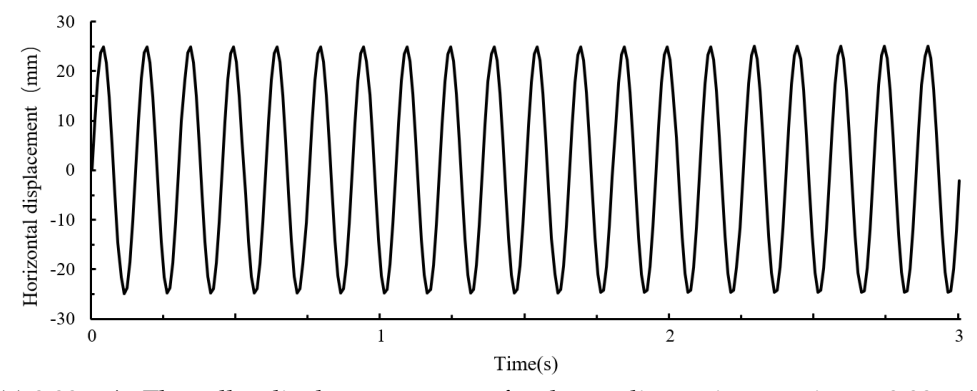
Using the same method, the displacement curves and pressure–strain values at the same node points were obtained for the testing platform when simulating operating speeds of 2.78 m/s and 3.33 m/s, respectively. The simulation results of the roller displacement curve are shown in Figure 11.



(a) 2.22 m/s: The roller displacement curve for the seeding unit operating at 2.22 m/s



(b) 2.78 m/s: The roller displacement curve for the seeding unit operating at 2.78 m/s



(c) 3.33 m/s: The roller displacement curve for the seeding unit operating at 3.33 m/s Fig. 11 - Simulation results of the roller displacement curve

The simulation results of the roller stress and strain are shown in Figure 12.

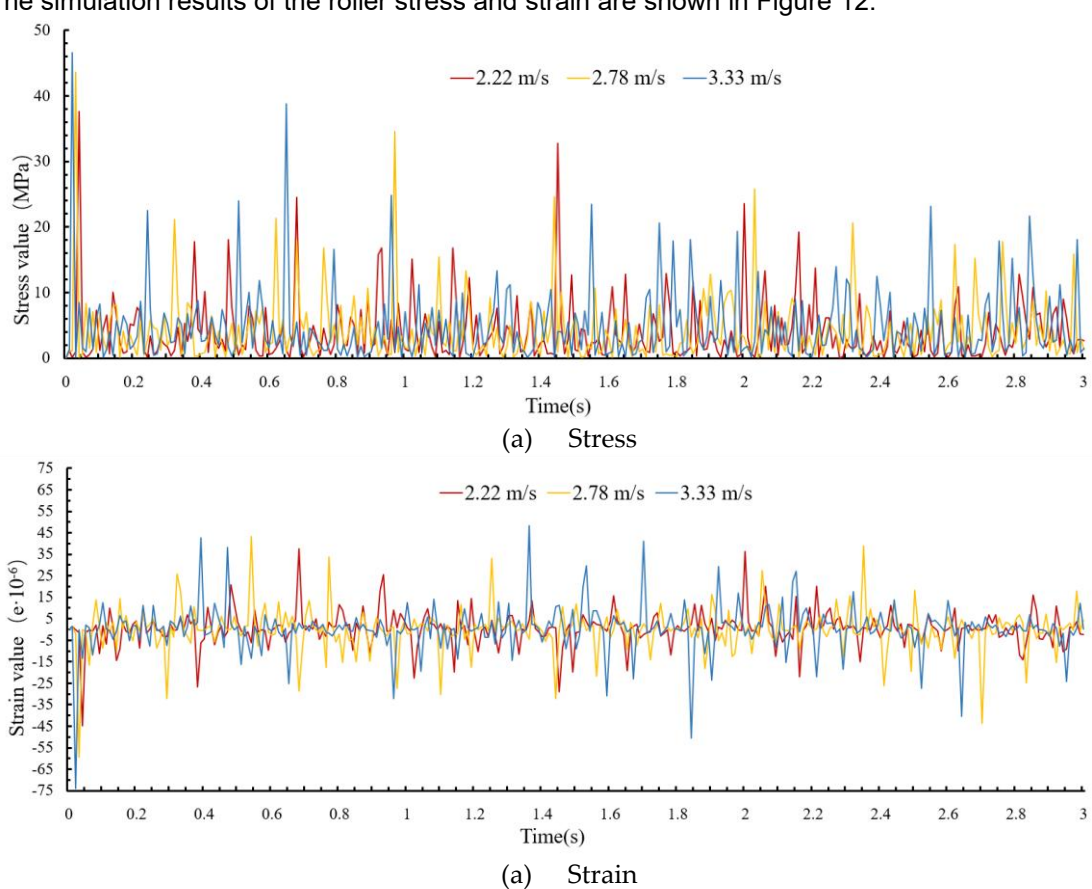


Fig. 12 - Simulation results of the roller stress and strain

Analysis of simulation test

From Figure 11, it can be observed that the hydraulic system can generate different pitching and lifting curves on the testing platform. The period and peak of the undulation curve at the roller's node point closely match the target values, and the extension and retraction of the piston rod remain within the stroke limits of the hydraulic system. Therefore, the simulation results indicate that the overall design of the pitching and lifting structure of the testing platform is reasonable.

From Figure 12, it can be seen that when the testing platform simulates different working conditions of the seeding unit, the stress and strain values at the roller's node point also exhibit periodic behavior. This occurs because the point is primarily influenced by the weight of the seeding unit and the supporting force exerted by the roller. During the cyclic lifting process of the testing platform, the hydraulic force in the cylinder periodically alters the magnitude of the support force acting on the roller, thereby affecting the stress and strain at this location. Furthermore, the period and peak values of stress and strain correspond to the period of the hydraulic force, which is directly related to the working speed of the simulated seeding unit. The higher the speed, the shorter the period and the greater the peak amplitude.

In Figure 12(a), the maximum stress value on the roller occurs during the startup phase when the testing platform simulates a speed of 3.33 m/s. This is because a larger hydraulic force is required during the startup of the hydraulic system, while the seeding unit has not yet generated sufficient upward inertial force, resulting in a greater effective load on the roller. The maximum stress value reaches 46.61 MPa, which is below the material's yield limit; therefore, the resulting stress will not cause structural damage and meets the operational safety requirements.

In Figure 12(b), the maximum strain on the roller also appears during the startup phase at a simulated speed of 3.33 m/s. At this stage, the node point on the roller is simultaneously subjected to an upward hydraulic force and a downward gravitational force from the seeding unit, making it more susceptible to compressive deformation. The maximum strain value is -73.99×10^{-6} , indicating a minor deformation that remains within safe limits and satisfies design requirements. Overall, the simulation results demonstrate that the transmission system of the testing platform is feasible and that its overall structural design is reasonable.

Results of bench test

Before conducting the test, ground contour data from the field test plot were collected. Using RTK-GNSS, measurements were taken from the same plot located in the demonstration field of Heilongjiang Bayi Agricultural University $(125^{\circ}09'57.6"\sim125^{\circ}10'8.4"E$, $46^{\circ}34'51.6"\sim46^{\circ}35'9.6"N$). Terrain data corresponding to operating speeds of 2.22 m/s, 2.78 m/s, and 3.33 m/s were collected and imported into the computer in text format (*Jing et al., 2019; Wang et al., 2023*).

The bench test was conducted in the Seeding Laboratory of Heilongjiang Bayi Agricultural University. Before testing, the Debont 1205 high-speed no-till corn planter unit, equipped with a spring-based profiling mechanism, was mounted on the testing platform. The angle sensor of the platform was fixed to the parallel upper link of the seeding unit, as shown in Figure 13.

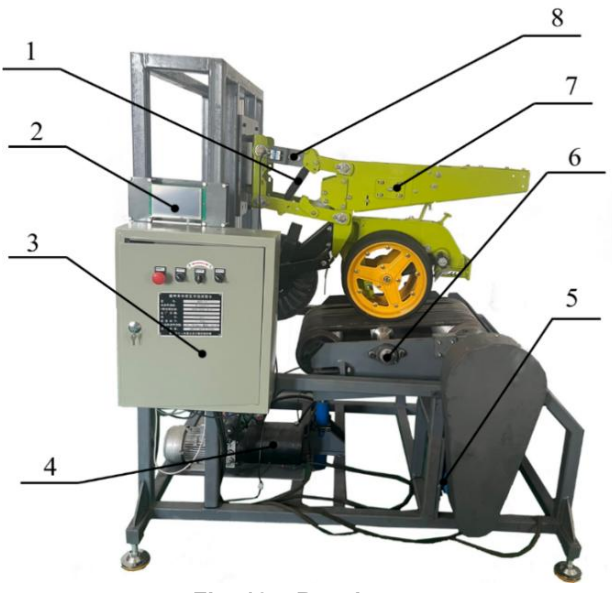


Fig. 13 – Bench test

Spring profiling mechanism;
 Vehicle-mounted computer;
 Button module;
 Hydraulic pump;
 Motor;
 Optical encoder;
 Debont 1205 high-speed no-till corn planter unit;
 Angle sensor

During the test, the curve data corresponding to the 2.22 m/s working speed were entered into the computer of the testing platform. The platform then simulated the working environment, and the detection results were output in graphical form. The profiling mechanism adjustment error P_t (m) and adjustment time T_t (s) detected by the testing platform were recorded. The initial and final segments, representing the acceleration and deceleration phases, were excluded from the data. Each test result was obtained as the average of multiple measurements.

The same procedure was applied to determine the adjustment error and adjustment time of the seeding unit at speeds of 2.78 m/s and 3.33 m/s. Each test was repeated three times to ensure accuracy.

To maintain consistent test conditions, the field experiment was conducted in the same demonstration field at Heilongjiang Bayi Agricultural University. A Massey Ferguson 1204 tractor was used as the towing power, as shown in Figure 14(a).

Before testing, the maximum undulation points within each 5-meter interval were marked, and an angle sensor was installed on the profiling mechanism to record real-time adjustment data. The preset sowing depth was 0.05 m, the test interval length was 100 m, and the working width was 1.9 m. The maximum undulation points within each 5-meter interval were marked, as shown in Figure 14(b).

During the field test, the operation was conducted at a forward speed of 2.22 m/s. A stopwatch was used to record the time when the unit reached each marked point. The time difference between this moment and the corresponding extreme value in the angle sensor data for that interval represented the actual adjustment time $T_f(s)$ of the profiling mechanism. In addition, a high-precision digital depth gauge (model XG-150) was used to measure the seeding depth at the start of each interval, and the actual adjustment error $P_f(m)$, defined as the difference between the preset and measured seeding depths, was calculated. The initial and final intervals (acceleration and deceleration phases) were excluded from the field data. The results were averaged.



(a) Field experiment process



(b) Data measurement process

Fig. 14 - Filed test

The same method was used to detect the adjustment error and adjustment time of the unit at 2.78 m/s and 3.33 m/s. Each test was repeated three times. The adjustment accuracy detection error and adjustment time detection error were calculated using the following formulas:

$$\Delta_P = \left| P_f - P_t \right| \tag{23}$$

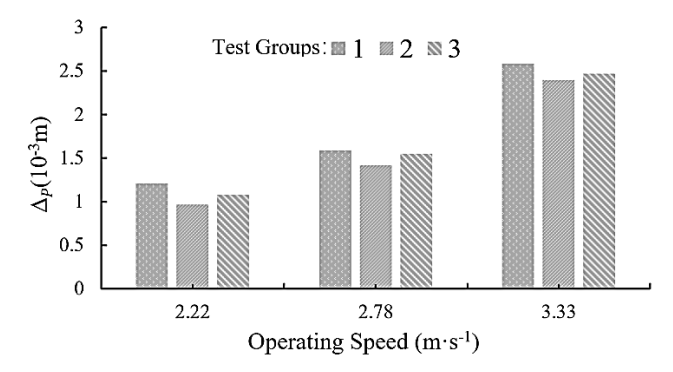
$$\Delta_T = \left| T_f - T_t \right| \tag{24}$$

The test results are shown in Table 3 and Figure 15.

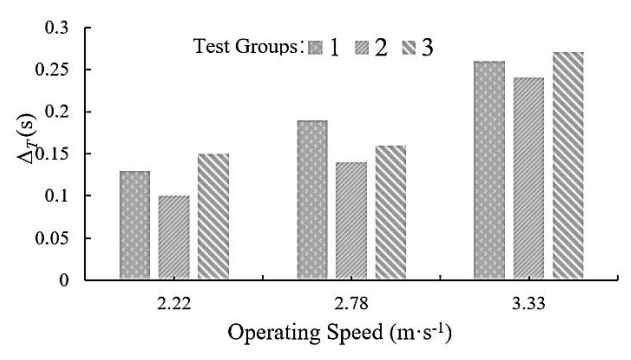
Test results

Table 3

Test Groups	Operating Speed (m·s·1)						
	2.22		2.78		3.33		
	$\Delta_P(m)$	$\Delta_T(s)$	$\Delta_P(m)$	$\Delta_T(s)$	$\Delta_P(m)$	$\Delta_T(s)$	
1	1.21×10⁻³	0.13	1.59×10⁻³	0.19	2.58×10⁻³	0.26	
2	0.97×10⁻³	0.10	1.42×10⁻³	0.14	2.40×10 ⁻³	0.24	
3	1.08×10⁻³	0.15	1.55×10 ⁻³	0.16	2.47×10⁻³	0.27	







(b) Δ_T vs. Speed: Adjustment Accuracy Error vs. Operating Speed

Fig. 15 - Adjustment Performance vs. Speed: Time and Accuracy Errors

Analysis of bench test

From the perspective of data variability across different test groups, the fluctuations in corresponding data points are relatively small, indicating that the testing platform exhibits stable detection accuracy.

From the overall trend of the results, the detection errors in both adjustment accuracy and adjustment time show a positive correlation with the operating speed of the seeding unit. This occurs because the spring profiling mechanism has difficulty maintaining high operational precision at elevated speeds, resulting in delayed adjustments. Consequently, both the detected adjustment errors and adjustment times increase noticeably in field and bench tests, thereby reducing the detection accuracy of the testing platform. In addition, when simulating high-speed working conditions, vibrations generated by the transmission system and elevation deviations caused by frequent piston extension and retraction further affect the detection precision of the platform.

In terms of the maximum observed values, the largest adjustment time detection error occurred in the third test of Group 3 at 3.33 m/s, with a value of 0.27 s, which is less than 0.50 s. The largest adjustment accuracy detection error occurred in the first test of Group 3 at 3.33 m/s, with a value of 2.58×10⁻³ m, which is less than 3×10⁻³ m. Therefore, the testing platform meets the performance requirements for detecting the profiling capability of the seeding unit, and the obtained results demonstrate high reliability.

CONCLUSIONS

- 1) To address the difficulty in accurately detecting the performance of seeding unit profiling mechanisms, a dedicated testing platform was designed. The platform employs a pitching structure capable of simulating ground undulations within a range of -12° to 9°. The transmission system achieves operating speeds from 2.09 to 5.35 m/s, while the monitoring system provides highly accurate data acquisition capabilities.
- 2) To realize the pitching function, a hydraulic system incorporating a pilot-operated electromagnetic relief valve as the core component was developed to work in coordination with the transmission system. Dynamic simulations at various operating speeds were conducted in RecurDyn to validate the curve simulation performance of the testing platform. The maximum stress on the roller was found to be $46.61 \, \text{MPa}$, and the maximum strain was -73.99×10^{-6} , confirming the rationality and structural integrity of the design.
- 3) To further verify the reliability of the testing platform, comparative experiments were performed using the average adjustment time and average adjustment accuracy as evaluation metrics. The results show that, at different operating speeds, the maximum average error between the adjustment time of the profiling mechanism measured on the testing platform and that obtained in the field was only 0.27 s. The maximum average error between the adjustment accuracy measured on the testing platform and that obtained in the field was 2.58×10⁻³ m. These findings demonstrate that the testing platform can accurately collect reliable data for evaluating the profiling performance of seeding units.

ACKNOWLEDGEMENT

This study was supported by the Key Research and Development Plan Project of Heilongjiang Province (2022ZX05B02).

REFERENCES

- [1] Bai, H., Fang, X., Wang, D., Yuan, Y., Zhou, L., Niu, K. (2020). Design and test of control system for seeding depth and compaction of corn precision planter (玉米播种机播深和压实度综合控制系统设计与试验). *Transactions of the Chinese Society for Agricultural Machinery*, 51(9), 61-72.
- [2] Bazzaz, M., Hossain, A., Timsina, J., Teixeira da Silva, J., Nuruzzaman, M. (2018). Growth, yield attributes and yield of irrigated spring wheat as influenced by sowing depth. *Open Agriculture*, 3(1), 72-83.
- [3] Cai, G., Li, H., Li, H., Wang, Q., He, J., Ni, J. (2011). Design of test-bed for automatic depth of furrow opening control system based on Atmega128 single chip microcomputer (基于 ATmega128 单片机的开沟深度自控系统试验台的设计). *Transactions of the CSAE*, 27(10), 11-16.
- [4] Cao, X.; Wang, Q.; Xu, D.; Huang, S.; Wang, X.; Wang, L. Design and Analysis of Pneumatic Downforce Regulating Device for No-Till Corn Planter [J]. *Agriculture* 2022, 12, 1513.
- [5] Ding, Q., You, Y., Xing, Q., Xu, G., Liang, L. (2022). Field bench test of seeding unit based on precise seeding depth control objective (基于精确播深控制目标的播种单体田间台架试验). *Transactions of the Chinese Society for Agricultural Machinery*, 53(11), 100-107.

- [6] Fu, W., Dong, J., Cong, Y., Lu, C., Gao, N., Zhang, J. (2017). Design and test of farmland-terrain simulation system for corn sowing depth control (基于玉米播深控制的农田地形模拟系统设计与试验). *Transactions of the Chinese Society for Agricultural Machinery*, 48(Supp.), 58-65.
- [7] Gao, Y., Zhai, C., Yang, S., Zhao, X., Wang, X., Zhao C. (2020). Development of CAN-based downforce and sowing depth monitoring and evaluation system for precision planter (精密播种机下压力和播深 CAN 总线监控与评价系统研究). *Transactions of the Chinese Society for Agricultural Machinery*, 51(6), 1528.
- [8] Helios, W., Jama-Rodzeńska, A., Serafin-Andrzejewska, M., Kotecki, A., Kozak, M., Zarzycki, P., Kuchar, L. (2021). Depth and sowing rate as factors affecting the development, plant density, height and yielding for two faba bean (Vicia faba L. var. minor) cultivars. *Agriculture*, 11, 820.
- [9] Hou, S., Xue, D., Cao, B., Chen, H., Han, Y. (2023). Design and test of a straw-clearing-depth self-adaptive control system of a front-mounted seedbed-preparation device. *Agriculture*, 13, 153.
- [10] Jiu, J., Xu, Q., Wu, M., Yang, G., Wu, M. (2023). Working characteristics and geometric calculation of friction-type V-belt drive (摩擦型 V 带传动的工作特点与几何计算). *Tractor & Farm Transporter*, 50(2), 77-82.
- [11] Jing, Y., Liu, G., Jin, Z. (2019). Topographic survey of farmland based on GNSS dual antenna combined with AHRS (GNSS 双天线结合 AHRS 测量农田地形). *Transactions of the CSAE*, 35(21), 166-174.
- [12] Liu, H., Zhang, W. (2022). Working performance of bidirectional profiling press device in hilly areas of Northeast China. *Agriculture*, 12, 1365.
- [13] Liu, W., Zeng, S., Chen, X. (2024). Design and experiment of adaptive profiling header based on multi-body dynamics–discrete element method coupling. *Agriculture*, 14, 105.
- [14] Ma, C., Yi, S., Tao, G., Li, Y., Wang, S., Wang, G., Gao, F. (2023). Research on receiving seeds performance of belt-type high-speed corn seed guiding device based on discrete element method. *Agriculture*, 13, 1085.
- [15] Ni, Y., Jin, C., Chen, M., Yuan, W., Qian, Z., Yang, T., Cai, Z. (2021). Computational model and adjustment system of header height of soybean harvesters based on soil-machine system. *Computers and Electronics in Agriculture*, 183, 105907.
- [16] Romaneckas, K., Pilipavičius, V., Šarauskis, E., (2009). Effect of sowing depth on emergence and crop establishment of sugar beet (Beta vulgaris L.). *Journal of Food, Agriculture & Environment*, 7(2), 571-575.
- [17] Sun, X., Chen, J., Wu, C., Xiao, D., Ye, J. (2021). Design and application of three-wheel non-circular synchronous belt drive test rig (三轮非圆同步带传动试验台设计与应用). *Transactions of the Chinese Society for Agricultural Machinery*, 52(1), 73-81.
- [18] Tang, Q., Wu, J., Jiang, L., Wu, C., Xiao, T., Jiang, T. (2021). Design and test of hydraulic profiling system for rape seedling combined transplanter (油菜耕整移栽联合作业机液压仿形系统设计与试验). *Transactions of the Chinese Society for Agricultural Machinery*, 52(11), 95-102.
- [19] Walne, C. H., Reddy, K. R. (2022). Temperature effects on the shoot and root growth, development, and biomass accumulation of corn (*Zea mays L.*). *Agriculture*, 12(4), 443.
- [20] Wang, P., Feng, D., Chen, G., He, J., Hu, L., Peng, J. (2023). Real-time 3D terrain measurement method and experiment in farmland leveling (农田精准平整过程中三维地形实时测量方法研究). *Transactions of the Chinese Society for Agricultural Machinery*, 54(3), 41-48.
- [21] Wang, T., Wang, T., Cui, H., Gong, Y., Tian, Su., Wang, R. (2021). Design and experiment of adjustable feeding straw bale-breaking and rubbing filament machine (喂入调节式秸秆破包揉丝机设计与试验). *Transactions of the Chinese Society for Agricultural Machinery*, 52(6), 148-158.
- [22] Yi, S., Li, Y., Chen, J., Wang, S., Zhao, B. (2024). Design and test of hydraulic active profiling mechanism for high-speed no-till corn planter (俯仰式播种单体仿形性能检测试验台设计与试验). *Transactions of the Chinese Society for Agricultural Machinery*, 55(02), 90-100.
- [23] Zhang, B., Zhang, W., Qi, L., Fu., Yu, L., Li, R., Zhao, Y., Ma, X. (2018). Information acquisition system of multipoint soil surface height variation for profiling mechanism of seeding unit of precision corn planter. *International Journal of Agricultural and Biological Engineering*, 11(6), 58-64.
- [24] Zhou, L., Ma, Y., Zhou, H., Niu, K., Zhao, B., Wei, L., Bai, S., Zheng, Y., Zhang, W. (2023). Design and test of sowing depth measurement and control system for no-till corn seeder based on integrated electrohydraulic drive. *Applied Sciences*, 13(10), 5823.